JOURNAL OF CATALYSIS **177,** 60–71 (1998)
ARTICLE NO. CA982039

The Transformations of n-Butane over Platinum-Promoted Mn-Aluminophosphate Molecular Sieves

A. Vieira,* M. A. Tovar,* C. Pfaff,* B. Méndez,* C. M. López,* F. J. Machado,* J. Goldwasser,*,[1] and M. M. Ramírez de Agudelo†

*Centro de Catálisis, Petróleo y Petroquímica, Escuela de Química, Facultad de Ciencias, Universidad Central de Venezuela, Apartado Postal 47102, Los Chaguaramos, Caracas 1020-A, Venezuela; and †INTEVEP, S.A., Apartado 76343, Caracas 1070-A, Venezuela

Received August 1, 1997; revised January 16, 1998; accepted February 9, 1998

The catalytic transformations of n-butane were performed over a platinum-promoted manganese-substituted aluminophosphate molecular sieve (Pt/MnAPO-11), and over a Pt promoted manganese-supported aluminophosphate molecular sieve (Pt/Mn/$AlPO_4$-11). For comparison purposes, the reactions were also carried out over a Pt-supported $AlPO_4$-11 molecular sieve (Pt/$AlPO_4$-11). X-ray diffraction (XRD) was used to determine the crystallographic structure of the unpromoted and Pt-promoted samples. Phosphorous 31-magic angle spinning-nuclear magnetic resonance (^{31}P MAS NMR) spectroscopy was used to study the possible ^{31}P–Mn(II) dipolar interaction. Brönsted and Lewis acidity were measured by pyridine chemisorption at different temperatures. Pt dispersions were determined by hydrogen chemisorption. CO chemisorption followed by IR spectroscopy was used to corroborate the dispersion measurements and to evaluate possible changes in the electronic density of the Pt phase. The catalytic results indicate higher yields (and selectivities) for the production of isobutane and isobutene over the Pt/MnAPO-11, compared with those observed over the Pt/Mn/$AlPO_4$-11 and Pt/$AlPO_4$-11 samples. Also, a severe decrease in the yield, in the selectivity and in the turnover frequency (TOF), for the formation of hydrocarbons with less than four carbon atoms, was observed for the Pt/MnAPO-11 system when compared with the Pt/Mn/$AlPO_4$-11 and Pt/$AlPO_4$-11 solids. A larger number of (moderate + strong) Brönsted acid sites was found for the MnAPO-11 solid compared to the Mn/$AlPO_4$-11 and $AlPO_4$-11 samples. For the last two solids, no Brönsted acidity was detected after evacuation of the catalyst at 623 K. ^{31}P MAS NMR results showed an increase in the intensity of the side bands, probably due to an anisotropic paramagnetic shift caused by a stronger dipolar interaction between the ^{31}P and the paramagnetic Mn(II) ions on the MnAPO-11 sample, when compared with the Mn/$AlPO_4$-11 solid. These results suggest a better dispersion of the manganese species on the MnAPO-11 solid, which would facilitate the above mentioned ^{31}P–Mn(II) interaction. The addition of platinum decreased the Lewis and Brönsted acidity for all the catalysts studied. The Pt dispersions were 68%, 59%, 49% for the Pt/$AlPO_4$-11, for the Pt/Mn/$AlPO_4$-11 and for the Pt/MnAPO-11 solids, respectively. The constant value obtained for the IR CO–Pt stretching frequency (Pt/$AlPO_4$-11 and Pt/MnAPO-11 samples) (ca 2067 cm^{-1}), as well as the drop in the Pt dispersion observed for the manganese containing solids, suggest an ensemble effect as responsible for the differences observed in the yield, selectivity, and TOF of formation of hydrocarbons with <C4. The higher yield and selectivity observed for the formation of iso-C4 and iso-C4= hydrocarbons over the Pt/MnAPO-11 solid, were accounted for in terms of the largest number of (moderate + strong) Brönsted acid sites found on this solid. The catalytic and characterization results suggest the incorporation of manganese into the molecular sieve structure, for the Pt/MnAPO-11 sample.

Key Words: **n-butane; Mn-aluminophosphates; molecular sieves; skeletal isomerization; dehydrogenation; platinum; Brönsted acidity; dehydroisomerization.**

INTRODUCTION

The new requirements for reformulated gasolines include the reduction of volatile compounds (particularly, linear C4 and C5 hydrocarbons), the decrease in the amount of olefins present in the gasoline and the addition of oxygenated compounds, which can act as octane enhancers (1, 2). Light unbranched paraffins are common byproducts found in refineries which can undergo dehydrogenation and skeletal isomerization, in different industrial processes (3–8), to yield branched olefins such as isobutene. The latter is a very valuable feedstock since it can react with methanol, generating methyl tert-butyl ether (MTBE), an important octane booster oxigenated fuel additive (1, 2). The dehydroisomerization of n-butane can, in principle, take place in a single process, thus decreasing the costs involved with two separate catalytic reactors. The reaction should be carried out under carefully controlled experimental conditions; e.g., the dehydrogenation reaction is favored at high temperatures but the skeletal isomerization is not (exothermic reaction). Highly selective catalytic systems are also necessary, in order to optimize the production of isobutene. Concomitantly, the direct transformation of n-butane can also

[1] To whom all correspondence should be addressed. E-mail: jgoldwas@strix.ciens.ucv.ve.

0021-9517/98 $25.00

yield appreciable amounts of isobutane, a valuable feedstock used in the production of isooctane (by reaction with n-butenes) (9).

The catalyts usually employed in the hydroisomerization of paraffins are bifunctional (10–13). These have hydrogenating–dehydrogenating (metallic) sites as well as moderate + strong acid centers necessary for the skeletal isomerization process.

Metal-substituted aluminophosphates (MeAPO's) (14–17), silicoaluminophosphates (SAPO's), and metal-substituted silicoaluminophosphates (MeAPSO's) (15–23), have been reported active for the skeletal isomerization of 1-butene. The high selectivity shown for the formation of isobutene over these solids has been associated with a specific acid site distribution and a particular crystal topology which minimize undesirable side reactions such as cracking and oligomerization.

Yang *et al.* (17) studied a series of MeAPO's for the skeletal isomerization of 1-butene. High selectivities for the latter were observed over Co, Zn, and Mn substituted aluminophosphates. Recently, we reported (15, 19) an increase in the acidity of a series of substituted MeAPO's-11 (Me = Mn, Cr, Fe), which caused an increase in the selectivity toward isobutene, compared to the unsubstituted $AlPO_4$-11 matrix. Different substitution models, depending on the metal oxidation state and stability of the metal species in the framework, were proposed to account for the results. In particular, for Mn(II), the model advanced by Gielgens *et al.* (14) was used to explain the increase in acidity observed when the metal was incorporated into the aluminophosphate structure, in agreement with other reports (24).

From the above discussion it follows that Mn-aluminophosphate molecular sieves meet the acidity and crystal topology requirements necessary for the skeletal isomerization of 1-butene. The main purpose of the present work is to study the direct dehydroisomerization of n-butane on a manganese-substituted aluminophosphate molecular sieve and on a manganese-supported aluminophosphate molecular sieve, promoted with a dehydrogenating agent (Pt), Pt/MnAPO-11, and Pt/Mn/$AlPO_4$-11, respectively. The results were compared with those obtained on a Pt promoted aluminophosphate molecular sieve (Pt/$AlPO_4$-11). The formation of isobutene and isobutane was evaluated, as well as the formation of other reaction products (C1–C3 hydrocarbons, n-butenes, etc.). X-ray diffraction, ^{31}P MAS NMR spectroscopy, acidity measurements (irreversibly chemisorbed pyridine, followed by infrared spectroscopy (IR)), CO chemisorption followed by IR spectroscopy, and metallic dispersion measurements (H_2 chemisorption), were used as characterization techniques. The results are discussed in terms of the possible mechanism of incorporation of manganese into the molecular sieve structure.

EXPERIMENTAL

I. Catalysts

The synthesis procedure for the $AlPO_4$-11 has been reported elsewhere (25). The gel molar composition was $Al_2O_3 : P_2O_5 : DPA : 50H_2O$.

The synthesis of the MnAPO-11 was performed according to the following scheme: The alumina source (pseudoboehmite, Catapal B from Vista Chemical Co.) was added to a diluted solution of phosphoric acid (Aldrich). The manganese promoter ($Mn(CH_3COO)_2 \cdot 4H_2O$, (Merck)) was then incorporated, followed by a stirring period of 2 h. The final step was the addition of the organic template, (di-n-propylamine (DPA) (Aldrich)), which was followed by a stirring period of 2 h. The gel molar composition was $0.9Al_2O_3 : P_2O_5 : 0.2MnO : DPA : 40H_2O$. A final crystallization temperature of 423 K and a crystallization time of 72 h were employed. The solid was first washed with distilled water and dried at 383 K for 16 h. The catalyst was then calcined under dry air at 783 K for 4 h in order to remove organic residues. A supported Mn/$AlPO_4$-11 catalyst was prepared by impregnating a sample of $AlPO_4$-11 with the same manganese promoter, using the incipient wetness technique (3.1 wt% Mn). This sample was then dried and calcined following the procedure described for the MnAPO-11 catalyst.

The Pt-promoted catalysts were prepared by impregnating the different calcined solids with $[Pt(NH_3)_4(NO_3)_2]$ (BDH, reagent grade) (26–28). The solids were dried under vacuum at 353 K. In order to decompose the Pt complex, the catalysts were calcined under a stream of dry air (30 cm^3/min), using the following procedure: The temperature was increased up to 423 K (5 K/min) followed by a 2-h period at the same temperature. The latter was then increased up to 573 K (5 K/min) and kept constant for 16 h. The Pt loading was 0.5 wt% Pt for all the Pt promoted solids.

For further experimental details dealing with the preparation and chemical analysis of the catalysts see Refs. (15, 25).

II. Procedures

X-ray diffractograms were recorded with a Philips diffractometer PW 1730 using Co-Kα radiation (λ = 1.790255 Å) operated at 30 KV, 20 mA and scanning speed of 2° (2θ/min).

^{31}P MAS NMR experiments were performed on a Bruker MSL spectrometer, operating at 121.44 MHz for ^{31}P. Other experimental details have been described previously (15).

Specific surface areas and microporous volumes were determined on a commercial Micromeritics ASAP 2400 surface area analyzer at liquid nitrogen temperature.

H_2 chemisorption experiments were performed in a conventional BET system similar to that used in Refs. (29–31).

Catalyst samples of approximately 0.2 g were placed in a glass microreactor and reduced *in situ* with pure H_2 (60 cm^3/min) for 2 h at 773 K. After evacuating the catalysts at the same temperature for 1 h, two adsorption isotherms were obtained at room temperature. The linear region of the first isotherm was extrapolated to zero pressure in order to calculate the amount of physisorbed and chemisorbed H_2. After an evacuation period of 1 h, the second isotherm was obtained. The same procedure (as in the first isotherm) was used to calculate the amount of physisorbed H_2. The irreversibly held H_2 was calculated from the difference between both values. A 1 : 1 H : Pt stoichiometry was assumed to calculate the metallic dispersion (H/Pt) (32, 33).

Infrared spectra were recorded at room temperature using a Perkin–Elmer 1760X FTIR spectrometer with a resolution of 2 cm^{-1}. The IR cell described previously (29–31) had a built-in furnace which was used to pretreat samples *in situ* at high temperatures. The cell could be attached to the BET vacuum system mentioned above. Samples were mounted in the cell as wafers having a thickness of approximately 10–20 mg/cm^2. Before the addition of CO or pyridine, the samples were reduced with pure H_2 (60 cm^3/min) at 773 K for 2 h. The catalysts were then evacuated ($P \leq 2 \cdot 10^{-5}$ Torr) for 1 h at the same temperature and cooled to the corresponding chemisorption temperature under vacuum.

The CO chemisorption experiments were performed as follows: After the corresponding pretreatment, purified CO (~50 Torr) was admitted into the IR cell at room temperature and the IR spectrum was registered. The sample was then evacuated ($P \leq 2 \cdot 10^{-5}$ Torr) for 1 h, and the spectrum recorded again. Integrated intensities (absorbances) were normalized to unit wafer thickness (mg/cm^2).

The pyridine chemisorption experiments were carried out by exposing the pretreated sample to 5 Torr of pyridine vapor for 1 h at 363 K. The wafer was then evacuated for 1 h at different temperatures before the spectra were recorded. The outgassing temperatures used in the present work were 443 and 623 K. The reason to use these temperatures is to arbitrarly define the following acidity regions: moderate + strong (sites retaining pyridine at 623 K) and total (weak + moderate + strong) (sites retaining pyridine at 443 K). Integrated intensities were normalized to unit wafer thickness (mg/cm^2).

n-Butane catalytic transformations were performed in a conventional continuous flow system (15, 21, 22) operated at atmospheric pressure. Preliminary experiments were carried out to determine the reaction conditions for maximum steady-state formation of isobutene. The reaction parameters used were: reaction temperature = 773 K, N_2 flow = 15 cm^3/min, H_2 flow = 15 cm^3/min, n-butane flow = 3 cm^3/min, weight of catalyst = 1.6 g (WHSV = 0.267 h^{-1}). The reaction products were analyzed by on-line gas chromatography, using a Hewlett–Packard 5890A chromatograph with a flame ionization detector. A fused silica KCl/Al_2O_3 column was used for separation purposes. The catalytic tests were performed after the solids were reduced with purified H_2 (60 cm^3/min) at 773 K for 2 h.

For discussion purposes, the skeletal isomerization of 1-butene was also carried out. The experimental conditions have been described previously (15, 21, 22) but will be repeated here for the sake of completion. A continuous flow system similar to the one employed in the n-butane experiments was used for the catalytic experiments. The reaction parameters used were: reaction temperature = 743 K, N_2 flow = 60 cm^3/min, 1-butene flow = 15 cm^3/min, weight of catalyst = 1 g. The catalytic tests were performed, for the calcined catalysts, after the solids were pretreated *in situ* (N_2, 60cc(STP)/min) overnight.

III. Data Treatment

n-Butane transformations. The total conversion (**X**) was calculated according to Eq. [1],

$$\mathbf{X} = \left\{ \left(\sum A_i \right) - A_{\text{n-butane}} \Big/ \sum A_i \right\} \times 100. \qquad [1]$$

For a reaction product (or set of products), the selectivity is defined by Eq. [2],

$$S_i = \left\{ A_i \Big/ \left(\sum A_i \right) - A_{\text{n-butane}} \right\} \times 100, \qquad [2]$$

where A_i is the corrected chromatographic area for a particular compound.

The catalytic yield (Y) for the different reaction products is defined by Eq. [3],

$$Y_i = S_i \times \mathbf{X}/100. \qquad [3]$$

The following selectivities and yields were determined: $S_{\text{iso-C4}}$, $Y_{\text{iso-C4}}$ (formation of isobutane); $S_{\text{n-C4=}}$, $Y_{\text{n-C4=}}$ (formation of n-butenes); $S_{\text{iso-C4=}}$, $Y_{\text{iso-C4=}}$ (formation of isobutene); $S_{<C4}$, $Y_{<C4}$ (formation of C1–C3 products). No other products were detected.

The turnover frequencies (TOF) for the formation of the different reaction products were calculated according to Eq. [4],

$$\text{TOF} = (4.99 \times 10^{-6} \times Y_i)/(\text{H/Pt}). \qquad [4]$$

TOF are expressed in molecules per second per surface Pt atom. The TOF for the formation of isobutene and isobutane over the Pt/MnAPO-11 solid were not calculated due to a possible bifunctional mechanism contribution., vide infra.

Skeletal isomerization of 1-butene. The total conversion (**X**) was calculated according to Eq. [5]

$$\mathbf{X} = \left\{ \left(\sum A_i \right) - A_{\text{1-butene}} \Big/ \sum A_i \right\} \times 100. \qquad [5]$$

For a reaction product (or set of products), the selectivity is defined by Eq. [6],

$$S_i = \left\{ A_i \Big/ \left(\sum A_i \right) - A_{1\text{-butene}} \right\} \times 100, \qquad [6]$$

where A_i has been defined above.

The following selectivities were determined: S_{iso} (skeletal isomerization); $S_{2\text{-}b}$ (double bond isomerization); S_{diene} (formation of butadiene); S_{crack} (formation of C1–C3 products); S_{C5+} (formation of hydrocarbons with five or more carbon atoms).

IV. Reagents

n-Butane and 1-butene were Matheson C. P. grade. Hydrogen was purified by passing it through a molecular sieve and commercial Deoxo traps to remove water and oxygen traces. CO (GIV) was purified according to Refs. (29, 31, 34). Pyridine (Aldrich, spectrophotometric grade) was degassed using the freeze-pump-thaw technique (35).

RESULTS

Table 1 shows some physicochemical properties of the solids used in the present work. The specific surface area (SSA) and microporosity values agree with other reports for solids having similar crystallographic structures (23, 25, 36). The addition of the platinum promoter decreases by ~15% the SSA and the microporous volume of the $AlPO_4$-11 and MnAPO-11 solids. The unit cell parameters, calculated before calcination, are in good agreement with those previously reported (37) for a body-centered orthorhombic unit cell of $AlPO_4$-11-like structures. However, the increase in the unit cell volume observed for the MnAPO-11 solid, compared to the $AlPO_4$-11 catalyst, should be noted.

Figure 1 shows the XRD diffractogram for the as-synthesized and calcined $AlPO_4$-11 sample and for the calcined

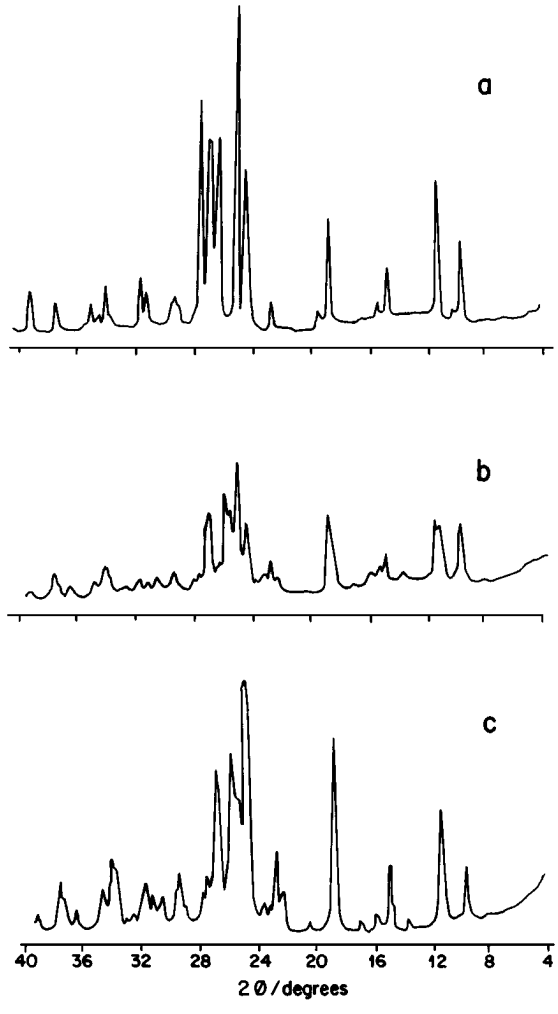

FIG. 1. X-ray diffractogram for the: (a) as-synthesized $AlPO_4$-11; (b) calcined $AlPO_4$-11; and (c) calcined Pt/$AlPO_4$-11 catalyst.

TABLE 1

Physicochemical Properties of the Different Solids Used in the Present Work

Catalyst	SSA/(m^2/g)[a]	Vμp/(cm^3/g)[b]	Molar composition (formula TO_2)	Unit cell parameters[c]		
				A	B	C
$AlPO_4$-11	162	0.051	$(Al_{0.52}P_{0.48})O_2$	18.67	13.33	8.39
MnAPO-11[d]	160	0.050	$(Al_{0.47}P_{0.48}Mn_{0.05})O_2$	18.79	13.52	8.46
Mn/$AlPO_4$-11[e]	145	0.045	$Mn/(Al_{0.52}P_{0.48})O_2$			
Pt/$AlPO_4$-11[f]	136	0.043	$Pt/(Al_{0.52}P_{0.48})O_2$			
Pt/MnAPO-11	134	0.042	$Pt/(Al_{0.47}P_{0.48}Mn_{0.05})O_2$			
Pt/Mn/$AlPO_4$-11	137	0.043	$Pt/Mn/(Al_{0.52}P_{0.48})O_2$			

[a] Specific surface area in m^2/g.
[b] Microporous volume in cm^3/g.
[c] Unit cell parameters in Å.
[d] Mn loading = 3.5 wt% Mn.
[e] Mn loading = 3.1 wt% Mn.
[f] The Pt loading for all the Pt promoted samples was 0.5 wt% Pt.

Pt/$AlPO_4$-11 solid. The diffractogram for the as-synthesized sample (Fig. 1a) shows a highly crystalline solid with $AlPO_4$-11 (AEL) structure, in agreement with the literature (15, 25, 36, 37). The major XRD changes observed for the calcined solid (Fig. 1b) have previously been reported (25, 38). They have been associated with a change in the crystal symmetry from a body-centered to a primitive unit cell as a result of water adsorption after calcination. The diffractogram for the Pt/$AlPO_4$-11 (Fig. 1c) solid, shows that the location of the main XRD peaks (25, 38) associated with the calcined $AlPO_4$-11 catalyst (Fig. 1b), remains unaltered after the addition of platinum to the calcined $AlPO_4$-11 solid. This result supports the fact that the addition of platinum does not change the crystallographic structure of the calcined $AlPO_4$-11 solid.

The XRD diffractograms for the as-synthezised and calcined MnAPO-11 and for the calcined Pt/$AlPO_4$-11 solids are shown in Fig. 2. The observed pattern for the as-synthezised solid (Fig. 2a) is very similar to the one observed for the as-synthezised $AlPO_4$-11 catalyst, typical of AEL structure. As with the $AlPO_4$-11 solid, the calcination–rehydration process generates significant changes in the XRD diffractogram (Fig. 2b). The latter is similar to the XRD diffractogram shown by the Pt/MnAPO-11 solid (Fig. 2c).

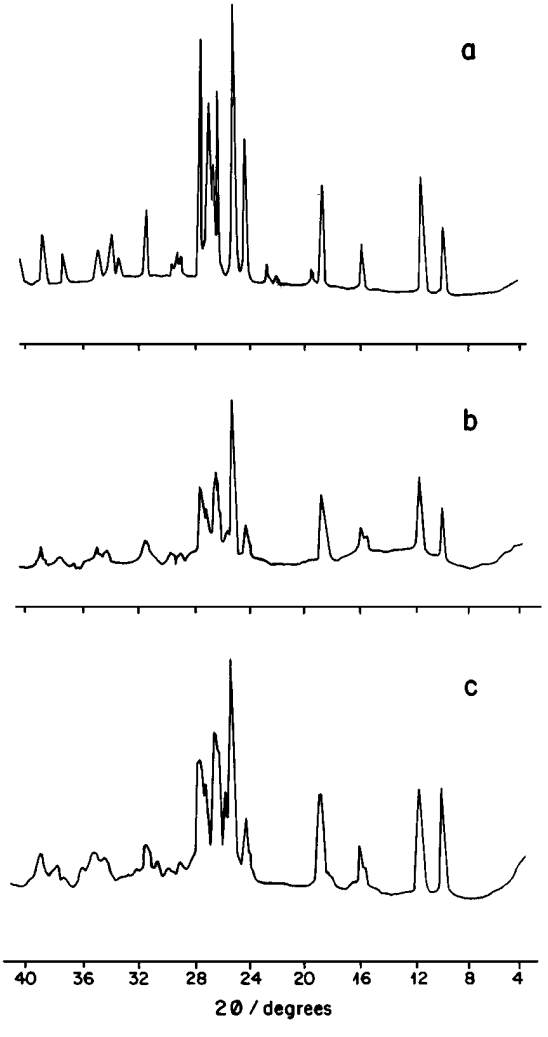

FIG. 2. X-ray diffractogram for the: (a) as-synthesized MnAPO-11; (b) calcined MnAPO-11; and (c) calcined Pt/MnAPO-11 catalyst.

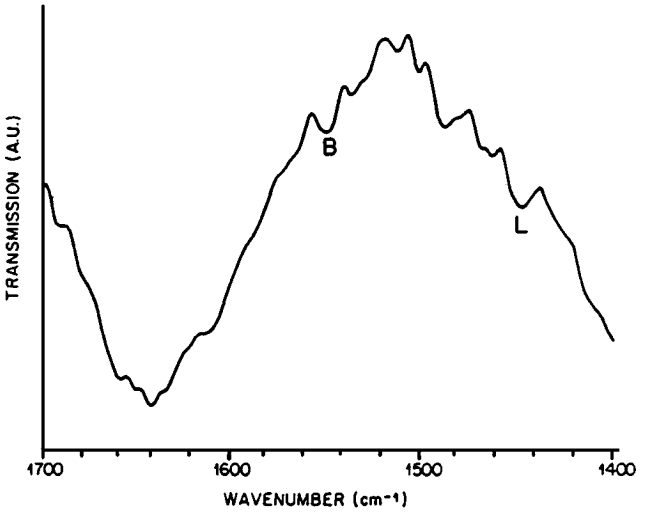

FIG. 3. Infrared spectrum of pyridine adsorbed on the oxidic MnAPO-11 sample after evacuation at 623 K. B and L stand for the bands diagnostic of Brönsted and Lewis bound pyridine, respectively.

The XRD results for the Mn/$AlPO_4$-11 and Pt/Mn/$AlPO_4$-11 were very similar to those reported for the calcined $AlPO_4$-11 (Fig. 1b). No Pt or Mn diffraction peaks were apparent in any of the solids studied in the present work.

Figure 3 shows the IR spectrum for the pyridine adsorption over the MnAPO-11 solid evacuated at 623 K. Only this spectrum is shown due to the similar nature of the other IR data. The spectrum was obtained by subtracting the contribution from the sample before the adsorption of pyridine. The two bands observed at ca 1450 cm^{-1} and ca 1548 cm^{-1} have previously been used in the literature (30, 35, 39) for estimating Lewis and Brönsted acidity on heterogeneous catalysts. The former corresponds to the 19b vibration of the Lewis bound pyridine. The band at ca 1548 cm^{-1} has been assigned to pyridine adsorbed on Brönsted acid sites. Table 2 summarizes the normalized integrated intensities for the IR bands due to Brönsted and Lewis bound pyridine for catalysts evacuated at 443 and 623 K. No pyridine adsorption occurring on Brönsted sites was detected for the $AlPO_4$-11 and for the Mn/$AlPO_4$-11 solids after evacuation at 623 K, in agreement with other reports (15) which showed the absence of (moderate + strong) Brönsted acid sites for the parent $AlPO_4$-11 solid. For the MnAPO-11 solid, however, the Brönsted-bound pyridine band, after evacuation at 623 K, was clearly present. It can also be seen that the addition

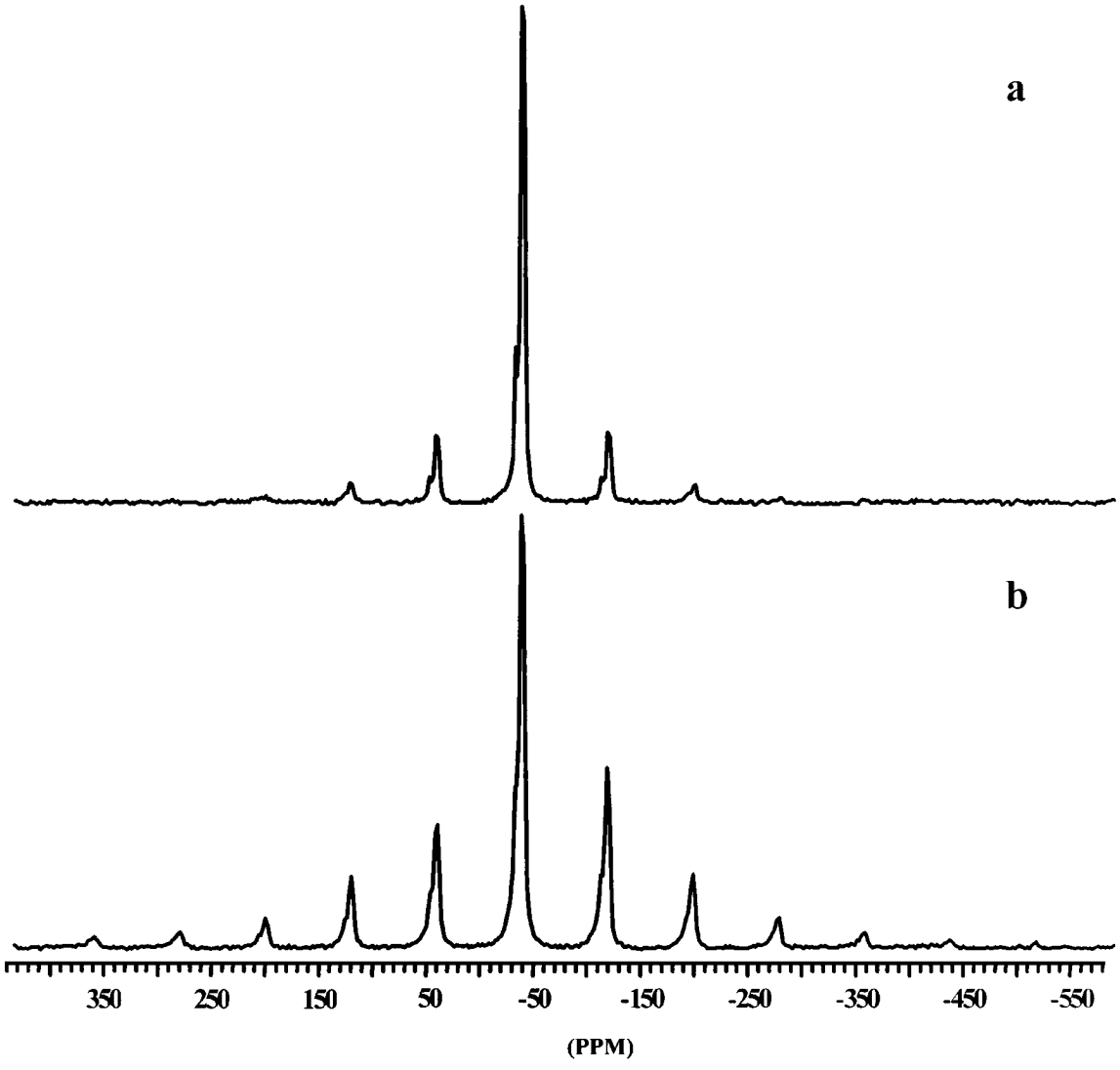

FIG. 4. ^{31}P MAS NMR spectra of: (a) calcined Mn/$AlPO_4$-11 solid; (b) calcined MnAPO-11 catalyst.

TABLE 2

Normalized Integrated Intensities for the 1548 cm^{-1} IR Band (Brönsted Bound Pyridine) and for the 1450 cm^{-1} Band (Lewis Bound Pyridine)[a]

	Evacuation temperature/K			
	443		623	
Catalyst	1548 cm^{-1}	1450 cm^{-1}	1548 cm^{-1}	1450 cm^{-1}
$AlPO_4$-11	2.8	4.2	n.d.[b]	2.4
MnAPO-11	2.5	2.9	1.5	2.1
Mn/$AlPO_4$-11	2.6	4.0	n.d.[b]	1.9
Pt/$AlPO_4$-11	2.5	3.8	n.d.[b]	1.9
Pt/MnAPO-11	2.2	2.4	1.2	1.8
Pt/Mn/$AlPO_4$-11	2.3	3.5	n.d.[b]	1.8

[a] For more details see text.
[b] n.d. = not detected.

of Pt to the MnAPO-11 catalyst causes, in particular, a slight decrease in the integrated intensity of the IR bands corresponding to (moderate + strong) Lewis and Brönsted sites, in agreement with reports on related systems (12, 40).

Figure 4 shows the ^{31}P MAS NMR spectra for the MnAPO-11 and Mn/$AlPO_4$-11 samples. It can be observed that for the substituted solid, the intensity of the side bands is strongly enhanced when compared with the supported material, in agreement with previous work (15, 47).

Figure 5 shows the IR spectra for the irreversible chemisorption of CO on the Pt/$AlPO_4$-11 and Pt/MnAPO-11 solids. Only one band at ca 2067 cm^{-1} was detected in the 1700–2100 cm^{-1} range. This band has previously been assigned (41–43) to a linear Pt–CO stretching vibration.

Table 3 summarizes the results for the hydrogen uptake and for the IR CO chemisorption experiments. No hydrogen chemisorption was detected for the $AlPO_4$-11 solid

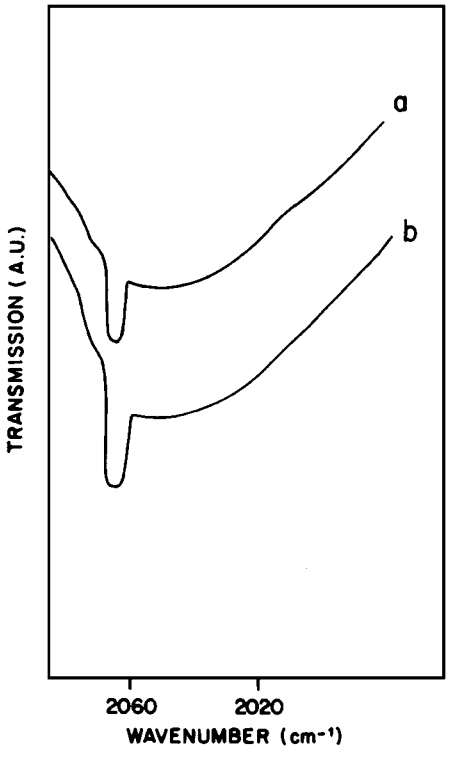

FIG. 5. Infrared spectra of irreversibly held carbon monoxide over Pt/MnAPO-11 (spectrum a) and over Pt/$AlPO_4$-11 (spectrum b).

while the MnAPO-11 and Mn/$AlPO_4$-11 samples did chemisorb a small amount of H_2. For the Pt promoted solids the uptake followed the sequence Pt/$AlPO_4$-11 > Pt/Mn/$AlPO_4$-11 > Pt/MnAPO-11 catalyst. The metallic dispersion (H/Pt ratio) for the Pt/MnAPO-11 and for the Pt/Mn/$AlPO_4$-11 solids was calculated, considering the total H_2 uptake for these catalysts without substracting the small amount of H_2 chemisorbed by the MnAPO-11 and Mn/$AlPO_4$-11 solids, respectively. The Pt dispersion was ~39% larger for the Pt/$AlPO_4$-11, compared to that observed for the Pt/MnAPO-11 solid. The integrated intensities for the irreversible CO chemisorption followed a similar trend; viz., the CO–Pt/$AlPO_4$-11 band was 37% more intense than the corresponding CO–Pt/MnAPO-11 band. The IR frequencies were the same within experimental error (2067 ± 1 cm^{-1}).

TABLE 3

H_2 Uptakes and IR Integrated Intensities for the CO–Pt Band[a]

Catalyst	H_2 uptake/ μmol/g	H/Pt	IR frequency/ cm^{-1}	Integrated intensity/A.U
$AlPO_4$-11	n.d.[b]	—	—	—
MnAPO-11	1.10	—	—	—
Mn/$AlPO_4$-11	1.22	—	—	—
Pt/$AlPO_4$-11	8.72	0.68	2067	10.9
Pt/MnAPO-11	6.28	0.49	2068	8.0
Pt/Mn/$AlPO_4$-11	7.56	0.59	—	—

[a] For more details see text.
[b] n.d. = not detected.

n-Butane catalytic tests were carried out over the $AlPO_4$-11, MnAPO-11, and Mn/$AlPO_4$-11 solids. The steady-state total conversion was always below 2%. The results for the transformation of n-butane over the Pt promoted solids are shown in Tables 4–9. No hydrocarbons with more than four carbon atoms were detected. The most striking feature is the dramatic decrease in the yield, selectivity, and TOF for the production of C1–C3 hydrocarbons on the Pt/MnAPO-11 compared to the Pt/$AlPO_4$-11 and Pt/Mn/$AlPO_4$-11 samples. When compared with the Pt/$AlPO_4$-11 sample, the supported Pt/Mn/$AlPO_4$-11 solid showed a smaller decrease in the TOF for the formation of C1–C3 hydrocarbons.

The catalytic results also indicate higher yields (and selectivities) for the production of isobutene and isobutane over the Pt/MnAPO-11 solid, compared with the Pt/$AlPO_4$-11 and Pt/Mn/$AlPO_4$-11 catalysts. Similar yields (and selectivities) for the production of both iso-C_4 products were observed over the Pt/$AlPO_4$-11 and Pt/Mn/$AlPO_4$-11 solids.

The TOF for the formation of n-butenes was larger on the Pt/Mn/$AlPO_4$-11 solid, particularly at high times-on-stream (TOS).

For discussion purposes, the catalytic results of the skeletal isomerization of 1-butene over the unpromoted supports ($AlPO_4$-11 and MnAPO-11) are shown in Tables 10 and 11. A small part of these results have been published previously (15). It can be seen that the MnAPO-11 catalyst is much more selective toward the formation of isobutene than the $AlPO_4$-11 solid. The latter, however, showed a higher selectivity for double bond isomerization, which is known to require weaker acid sites than those needed for the skeletal isomerization (44). Neither catalyst showed any significant activity for dehydrogenation, cracking, or oligomerization reactions. The results for the Mn/$AlPO_4$-11 solid were almost identical to those obtained over the $AlPO_4$-11 catalyst.

DISCUSSION

The following characterization results suggest the incorporation of manganese into the aluminophosphate molecular sieve structure, for the MnAPO-11 catalyst:

1. The unit cell volume is smaller for the $AlPO_4$-11 solid than for the MnAPO-11 catalyst (Table 1). This can be understood in terms of the difference in bond length found for Al–O (1.75 Å) compared to Mn–O (2.02 Å).

2. The increased (moderate + strong) Brönsted acidity shown by the MnAPO-11 catalyst (Table 2), compared with the $AlPO_4$-11 and with the supported Mn/$AlPO_4$-11 solids. Particularly, the difference in acidity between the substituted and supported manganese catalysts is significant since the latter should contain predominantly extra-framework manganese species. The appearance of these species does

TABLE 4

Product Distribution for the Transformations of n-Butane over Pt/$AlPO_4$-11[a]

TOS[b]	X	$S_{iso\text{-}C4}$	$S_{iso\text{-}C4=}$	$S_{n\text{-}C4=}$	$S_{<C4}$	$Y_{iso\text{-}C4}$	$Y_{iso\text{-}C4=}$	$Y_{n\text{-}C4=}$	$Y_{<C4}$
45	52.5	12.2	6.1	18.7	62.9	6.4	3.2	9.8	33.1
60	50.2	12.3	6.5	21.1	60.0	6.2	3.3	10.6	30.2
90	47.2	11.9	6.9	25.0	56.2	5.6	3.3	11.8	26.5
120	45.5	11.6	7.4	28.0	53.0	5.3	3.4	12.7	24.1
150	41.6	12.2	6.9	29.5	51.4	5.1	2.9	12.3	21.4
180	41.7	11.6	7.2	30.3	50.8	4.8	3.0	12.6	21.2
240	43.5	11.1	7.5	32.4	49.1	4.8	3.3	14.1	21.3
300	40.1	10.3	7.7	35.6	46.4	4.2	3.1	14.3	18.6

[a] The reaction parameters used were: reaction temperature = 773 K, N_2 flow = 15 cm^3/min, H_2 flow = 15 cm^3/min, n-butane flow = 3 cm^3/min, weight of catalyst = 1.6 g (WHSV = 0.267 h^{-1}).
[b] Time on-stream/min.

not create new (moderate + strong) Brönsted acid sites, compared with the $AlPO_4$-11 sample. The situation with the MnAPO-11 solid is clearly different. This can be accounted for in terms of the incorporation of Mn(II) into the aluminophosphate structure (MnAPO-11) by replacement of an Al(III) cation, as proposed by Gielgens *et al.* (14). According to these ideas, Mn(II) would be incorporated into the molecular sieve framework generating one P–OH group per each metal ion, thus increasing the number of acid sites. The interaction of the metal ions (Lewis centers) with the P–OH groups (Brönsted sites) may increase the strength of the latter, as shown for related systems (15, 21, 22). The presence of (moderate + strong) Lewis sites on the $AlPO_4$-11 solid has been attributed to structural breakage after calcination to yield defective Al sites (15).

3. ^{31}P MAS NMR spectra (Fig. 4), which show different behavior for the manganese species present on the substituted and supported samples, in accordance with previous reports (15). An anisotropic paramagnetic shift due to a ^{31}P-paramagnetic Mn(II) dipolar interaction for the MnAPO-11 catalyst has been suggested (15, 47) to account for the observed differences in the intensities of the side bands. These results suggest a better dispersion of the manganese species on the MnAPO-11 solid, which would facilitate the above-mentioned ^{31}P–Mn(II) interaction.

In addition, previous ESR (15) results, showed different manganese chemical environments for a MnAlPO-11 sample (0.1 wt% Mn) and for a Mn supported $AlPO_4$–11 solid (0.1 wt% Mn), in accordance with Brouet *et al.* (45, 46). Although the Mn wt% is much lower than those used in the present work, these results should be taken as existing examples for the possible incorporation of manganese into $AlPO_4$-11 molecular sieve frameworks. However, these ESR results by themselves, do not provide independent support for the incorporation of manganese into the molecular sieve framework for the MnAPO-11 solid used in the present work, due to the differences in Mn loading. Unfortunately, it was impossible to resolve the X-band ESR spectrum for catalysts with higher manganese contents (15), including those used in the present study.

The above-mentioned results (points 1 through 3), support the assumption of Mn(II) being incorporated into the aluminophosphate molecular sieve structure, in agreement with other studies (14–16, 45, 48). However, the presence of some extra-framework manganese species on the substituted solid cannot be ruled out; viz, our data does not allow us to conclude that all the manganese is incorporated into the molecular sieve structure MnAPO-11.

The addition of Pt decreases the acidity of the catalysts (Brönsted and Lewis sites), in agreement with results obtained over Pt/SAPO-11 catalysts (12, 40). The dispersion, measured by the irreversibly chemisorbed hydrogen, was 49% for the Pt/MnAPO-11, 59% for the Pt/Mn/$AlPO_4$-11, and 68% for the Pt/$AlPO_4$-11 solid. These values were calculated by taking into account the total irreversibly held hydrogen, without substracting the possible contribution of the MnAPO-11 and Mn/$AlPO_4$-11 solids. In order to establish the validity of this argument, the CO chemisorption was performed on the Pt/$AlPO_4$-11 and Pt/MnAPO-11 samples and followed by IR spectroscopy. The intensity results for the ca 2067 cm^{-1} band, which has unambiguously

TABLE 5

Turnover Frequencies[a] for the Transformations of n-Butane over Pt/$AlPO_4$-11

TOS[b]	X	$TOF_{iso\text{-}C4}$	$TOF_{iso\text{-}C4=}$	$TOF_{n\text{-}C4=}$	$TOF_{<C4}$
45	52.5	4.7	2.3	7.2	24.3
60	50.2	4.6	2.4	7.8	22.1
90	47.2	4.1	2.4	8.7	19.5
120	45.5	3.9	2.5	9.3	17.7
150	41.6	3.7	2.1	9.0	15.7
180	41.7	3.5	2.2	9.3	15.6
240	43.5	3.5	2.4	10.3	15.6
300	40.1	3.0	2.3	10.5	13.6

[a] Turnover frequencies/mol/s per surface Pt atom $\times 1 \cdot 10^{-5}$.
[b] Time on-stream/min.

TABLE 6

Product Distribution for the Transformations of n-Butane over Pt/MnAPO-11[a]

TOS[b]	X	$S_{iso\text{-}C4}$	$S_{iso\text{-}C4=}$	$S_{n\text{-}C4=}$	$S_{<C4}$	$Y_{iso\text{-}C4}$	$Y_{iso\text{-}C4=}$	$Y_{n\text{-}C4=}$	$Y_{<C4}$
45	31.0	31.8	19.7	41.3	7.2	9.9	6.1	12.8	2.2
60	30.8	30.5	19.8	43.2	6.5	9.4	6.1	13.3	2.0
90	29.3	29.1	19.9	44.7	6.3	8.5	5.8	13.1	1.8
120	28.4	28.1	20.1	46.3	5.5	8.0	5.7	13.2	1.6
150	27.8	28.9	19.7	45.8	5.6	8.0	5.5	12.7	1.6
180	27.8	27.4	20.1	47.3	5.2	7.6	5.6	13.1	1.4
240	26.4	24.9	20.6	49.7	4.8	6.6	5.4	13.1	1.3
300	25.7	23.2	20.9	51.4	4.5	6.0	5.4	13.2	1.2

[a] The reaction parameters used were: reaction temperature = 773 K, N_2 flow = 15 cm^3/min, H_2 flow = 15 cm^3/min, n-butane flow = 3 cm^3/min, weight of catalyst = 1.6 g (WHSV = 0.267 h^{-1}).

[b] Time on-stream/min.

been attributed to a linear Pt–CO interaction (41–43), show that the platinum in the $Pt/AlPO_4$-11 solid is 37% more dispersed than in the Pt/MnAPO-11 catalyst. This value arises from the ratio of the integrated intensities, assuming that the molar extinction coefficients for both bands are the same. This result is virtually identical to the one obtained by H_2 chemisorption (without substracting the MnAPO-11 contribution). Had the latter been substracted, the Pt dispersion in the Pt/MnAPO-11 solid would have been ~40% and the Pt in the $Pt/AlPO_4$-11 solid would have been 70% more dispersed than that of Pt/MnAPO-11. As shown, this result does not agree with the IR–CO chemisorption experiments.

Besides the numerical implications, the above results show that the presence of manganese (Pt/MnAPO-11) decreases the amount of hydrogen held by the platinum particles and that seemingly no significant hydrogen chemisorption occurs on the manganese species in the presence of metallic platinum. A close proximity between Pt and manganese species can, therefore, be suggested. This will be supported by the catalytic results, *vide infra*.

The results for the n-butane transformations reported in Tables 4–9 are consistent with the acidity and dispersion measurements. The most striking difference is the dramatic decrease in the TOF for the formation of C1–C3 hydrocarbons, unwanted side reaction, for the Pt/MnAPO-11 solid compared with the $Pt/AlPO_4$-11 and $Pt/Mn/AlPO_4$-11 catalysts. Since neither one of the last two solids has the acid strength (moderate + strong Brönsted acid sites) needed to carry out the acid cracking of n-butane and that the $AlPO_4$-11 and $Mn/AlPO_4$-11 catalysts are extremely poor catalysts for cracking and for the skeletal isomerization of 1-butene, it can be safely assumed that the C–C bond breakage occurs on the Pt surface of the $Pt/AlPO_4$-11 and $Pt/Mn/AlPO_4$-11 solids (hydrogenolysis reaction). The latter has been thoroughly investigated (49–52) over a variety of metallic surfaces. It is now widely accepted that this reaction is structure sensitive and that metallic ensembles over a certain size are needed for the reaction to occur. The decrease in the TOF for the hydrogenolysis reaction observed for the Pt/MnAPO-11 can, in principle, be attributed to an ensemble effect, an electronic effect, or to both. The constant value for the CO frequency (ca 2067 cm^{-1}) suggests that the Pt electron density (43) is quite similar in both solids ($Pt/AlPO_4$-11 and Pt/MnAPO-11); viz., the electronic properties of the Pt particles are not significantly affected by the presence of the manganese species. Therefore, our results suggest that the decrease in the TOF for the hydrogenolysis reaction is due to an ensemble effect. The latter is supported by the decrease in the Pt dispersion (observed for the Pt/MnAPO-11 solid) and it is made possible by the close proximity between Pt crystals and well dispersed manganese species discussed above.

As observed, the TOF for the hydrogenolysis reaction on the supported $Pt/Mn/AlPO_4$-11 catalyst is also smaller than that observed for the $Pt/AlPO_4$-11; however, the decrease is much smaller than that observed for the Pt/MnAPO-11 solid. A possible explanation could be that, in the case of the supported catalyst, the extra-framework manganese

TABLE 7

Turnover Frequencies[a] for the Transformations of n-Butane over Pt/MnAPO-11

TOS[b]	X	$TOF_{n\text{-}C4=}$	$TOF_{<C4}$
45	31.0	13.0	2.3
60	30.8	14.0	2.0
90	29.3	13.0	1.9
120	28.4	13.0	1.6
150	27.8	13.0	1.6
180	27.8	13.0	1.5
240	26.4	13.0	1.3
300	25.7	13.0	1.2

[a] Turnover frequencies/mol/s per surface Pt atom $\times 1 \cdot 10^{-5}$.

[b] Time on-stream/min.

TABLE 8

Product Distribution for the Transformations of n-Butane over Pt/Mn/$AlPO_4$-11[a]

TOS[b]	X	$S_{iso\text{-}C4}$	$S_{iso\text{-}C4=}$	$S_{n\text{-}C4=}$	$S_{<C4}$	$Y_{iso\text{-}C4}$	$Y_{iso\text{-}C4=}$	$Y_{n\text{-}C4=}$	$Y_{<C4}$
30	52.7	11.9	8.0	33.3	46.7	6.3	4.2	17.6	24.7
60	46.5	11.1	6.3	41.5	41.1	5.2	2.9	19.3	19.1
90	45.0	10.8	7.4	43.6	38.2	4.9	3.3	19.6	17.2
120	43.6	10.2	7.5	47.1	35.1	4.5	3.3	20.6	15.4
150	43.3	9.6	6.8	47.6	36.0	4.2	2.9	20.6	15.6
180	43.0	9.4	7.2	48.6	34.8	4.0	3.1	20.9	15.0
300	41.1	8.5	7.1	53.0	31.4	3.5	2.9	21.8	12.9

[a] The reaction parameters used were: reaction temperature = 773 K, N_2 flow = 15 cm^3/min, H_2 flow = 15 cm^3/min, n-butane flow = 3 cm^3/min, weight of catalyst = 1.6 g (WHSV = 0.267 h^{-1}).
[b] Time on-stream/min.

species are poorly dispersed (compared with the substituted solid), thus decreasing the likelihood of manganese species "seeing" the platinum particles. The difference in Pt dispersion between the supported and substituted molecular sieves, as well as the NMR results obtained for the MnAPO-11 and Mn/$AlPO_4$-11 solids, support the above ideas.

Another important difference observed is that the $S_{i\text{-}C4}$ and $S_{i\text{-}C4=}$ obtained for the Pt/MnAPO-11 catalyst are considerably higher than those obtained on the Pt/$AlPO_4$-11 and Pt/Mn/$AlPO_4$-11 solids. Skeletal isomerization of paraffins over heterogeneous catalysts is known to take place by either acid catalysis (53–55) or by a metal-assisted process (51, 52). Particularly, Pt has been shown to be extremely active for the isomerization process. Due to the lack of required acidity, mentioned above, the only possible way for the Pt/$AlPO_4$-11 and Pt/Mn/$AlPO_4$-11 solids to catalyze the skeletal isomerization of n-butane is through a process occurring over the Pt surface (probably, via a bond shift mechanism (51)). The isobutane produced can then be partially dehydrogenated to form isobutene.

The interpretation of the results obtained on the Pt/MnAPO-11 catalyst is more complicated due to the presence of (moderate + strong) Brönsted acid sites which are able to perform the skeletal isomerization of the n-butenes (Table 11). In this case, in addition to the isomerization–dehydrogenation process carried out over metallic centers, the conventional bifunctional mechanism can also take place to produce isobutene + isobutane (10–13). This mechanism includes: dehydrogenation of n-butane to form n-butenes, skeletal isomerization of the olefin over (moderate + strong) Brönsted acid sites to yield isobutene, followed by a hydrogenation step to form isobutane. Since the MnAPO-11 solid is more active for the skeletal isomerization of 1-butene than the $AlPO_4$-11 and Mn/$AlPO_4$-11 systems, the possibility of having a contribution towards the formation of iso-C4= (and iso-C4) from a bifunctional mechanism has to be considered. Again, the difference in behavior between the Pt/MnAPO-11 and Pt/Mn/$AlPO_4$-11 is evident.

Finally, the fact that no hydrocarbons with more than four carbon atoms were observed throughout the n-butane–H_2 experiments deserves a comment concerning the role of C8 intermediates (bimolecular mechanism (56–58)) in the formation of isobutene and isobutane over the Pt/MnAPO-11 solid. Previous work (1-butene skeletal isomerization) on manganese-substituted aluminophosphate molecular sieves (14) have shown that the formation of branched C8 intermediates in the Mn−$AlPO_4$-11 pores is difficult, probably due to the restrictions imposed by the particular pore geometry of these solids. Had the formation of the C8

TABLE 9

Turnover Frequencies[a] for the Transformations of n-Butane over Pt/Mn/$AlPO_4$-11

TOS[b]	X	$TOF_{iso\text{-}C4}$	$TOF_{iso\text{-}C4=}$	$TOF_{n\text{-}C4=}$	$TOF_{<C4}$
30	52.7	5.3	3.6	14.8	20.9
60	46.5	4.4	2.5	16.3	16.1
90	45.0	4.1	2.8	16.6	14.5
120	43.6	3.8	2.8	17.4	13.0
150	43.3	3.6	2.5	17.4	13.2
180	43.0	3.4	2.6	17.7	12.7
300	41.1	3.0	2.4	18.4	10.9

[a] Turnover frequencies/mol/s per surface Pt atom $\times 1 \cdot 10^{-5}$.
[b] Time on-stream/min.

TABLE 10

Product Distribution for the Transformations of 1-Butene over $AlPO_4$-11[a]

TOS[b]	X	S_{iso}	$S_{2\text{-}b}$	S_{diene}	S_{C5+}	S_{crack}
30	71.7	3.2	95.6	0.0	0.3	0.8
90	71.6	2.8	96.5	0.0	0.1	0.6
150	71.5	2.6	96.6	0.0	0.1	0.6
210	71.5	2.3	96.7	0.0	0.2	0.7
270	71.3	2.3	96.8	0.0	0.1	0.7
330	71.3	2.1	97.2	0.0	0.1	0.6

[a] The reaction parameters used were: reaction temperature = 743 K, N_2 flow = 60 cm^3/min, 1-butene flow = 15 cm^3/min, weight of catalyst = 1 g.
[b] Time on-stream/min.

TABLE 11

Product Distribution for the Transformations of 1-Butene over MnAPO-11[a]

TOS[b]	X	S_{iso}	$S_{2\text{-}b}$	S_{diene}	S_{C5+}	S_{crack}
30	84.4	28.5	69.4	0.1	1.0	1.0
90	83.8	26.2	72.0	0.1	1.0	0.7
150	78.5	34.9	62.9	0.1	1.2	0.9
210	77.5	34.9	63.0	0.1	1.1	0.9
270	83.0	23.1	75.5	0.1	0.8	0.6
330	82.6	22.4	76.4	0.1	0.6	0.6

[a] The reaction parameters used were: reaction temperature = 743 K, N_2 flow = 60 cm^3/min, 1-butene flow = 15 cm^3/min, weight of catalyst = 1 g.
[b] Time on-stream/min.

intermediate been facile, a wider product distribution, including C5 hydrocarbons, would have been obtained. The latter was not the case in the present work. The C8 intermediate, however, has been suggested as a key intermediate for the skeletal isomerization of n-butane over other solid acids with a wider distribution of pore sizes (less geometrical restrictions for the formation of the C8 intermediate), e.g., ZrO_2–SO_4 based catalysts (59–64).

CONCLUSIONS

The catalytic transformations of n-butane were performed over a platinum-promoted manganese-substituted aluminophosphate molecular sieve (Pt/MnAPO-11), and over a Pt-promoted manganese-supported aluminophosphate molecular sieve (Pt/Mn/$AlPO_4$-11). For comparison purposes, the reactions were also carried out over a Pt-supported $AlPO_4$-11 molecular sieve (Pt/$AlPO_4$-11). The catalytic results indicate higher yields and selectivities for the production of isobutane and isobutene over the Pt/MnAPO-11. A severe decrease in the yield, selectivity, and TOF of formation of hydrocarbons with less than four carbon atoms (undesirable side reaction) was also observed for the Pt/MnAPO-11 system, compared with the Pt/$AlPO_4$-11 and Pt/Mn/$AlPO_4$-11 systems.

Acidity was measured by pyridine chemisorption at different temperatures. A larger number of (moderate + strong) Brönsted acid sites was found for the MnAPO-11 solid, compared with the $AlPO_4$-11 and Mn/$AlPO_4$-11 samples. ^{31}P MAS NMR results showed an increase in the intensity of the side bands, probably due to an anisotropic paramagnetic shift caused by a stronger dipolar interaction between the ^{31}P and the paramagnetic Mn(II) ions on the MnAPO-11 sample, when compared with the Mn/$AlPO_4$-11 solid. These results suggest a better dispersion of the manganese species on the MnAPO-11 solid, which would facilitate the above-mentioned ^{31}P–Mn(II) interaction.

The addition of platinum decreased the acidity. Pt dispersions were measured by hydrogen chemisorption. CO chemisorption followed by IR spectroscopy was used, partially, to corroborate the dispersion measurements. The Pt dispersions were 68%, 59%, and 49% for the Pt/$AlPO_4$-11, Pt/Mn/$AlPO_4$-11, and Pt/MnAPO-11 solids, respectively. The constant value obtained for the IR CO–Pt stretching frequency over the Pt/$AlPO_4$-11 and Pt/MnAPO-11 solids ($\sim$2067 cm^{-1}), as well as the drop in the Pt dispersion for the manganese-containing samples, particularly Pt/MnAPO-11, suggest an ensemble effect as responsible for the differences observed in the yield of formation of hydrocarbons with less than four carbon atoms. The higher yield and selectivity observed for the formation of iso-C4 and iso-C4= hydrocarbons over the Pt/MnAPO-11 solid was accounted for in terms of the largest number of (moderate + strong) Brönsted acid sites found on this solid.

The catalytic and characterization results suggest the incorporation of manganese into the molecular sieve structure for the Pt/MnAPO-11 sample.

ACKNOWLEDGMENT

The authors are grateful to Consejo Nacional de Investigaciones Científicas y Tecnológicas (CONICIT) for financial support through Grant RPI-10001.

REFERENCES

1. Simon, M. W., Suib, S. L., and O'Young, C.-L., *J. Catal.* **147**, 484 (1994).
2. Maxwell, I. E., and Naber, J. E., *Catal. Lett.* **12**, 105 (1992).
3. Cornelius, E. B., and Koester, D. W., U.S. Patent 3,665,049 (1972).
4. Tomezsco, E. S., U.S. Patent 3,697,614 (1972).
5. Buonomo, F., Jezzi, R., Notari, B., and Kotelnikov, G. R., U.K. Patent GB 2,177,317A (1987).
6. Kuhlman, E. J., Pascoe, J. R., and Thom, C. J., U.S. Patent 5,463,160 (1995).
7. Apellan, M. R., Rahmim, I., Fung, A. S., and Huss, A., U.S. Patent 5,321,194 (1994).
8. Barger, P. T., Patton, R. L., Lesch, D. A., Bauer, L. J., and Gajda, G. J., U.S. Patent 5,365,008 (1996).
9. Pines, H., "The Chemistry of Catalytic Hydrocarbon Conversions." Academic Press, New York, 1981.
10. Mills, G. A., Heinemann, H., Milliken, T. H., and Oblad, A. G., *Ind. Eng. Chem.* **45**, 134 (1953). [Sinfelt, J. H., Hurwitz, H., and Rohrer, J. C., *J. Phys. Chem.* **64**, 892 (1960); Weisz, P. B., *Adv. Catal.* **13**, 137 (1962); Alvarez, F., Ribeiro, F. R., Giannetto, G., Chevalier, F., Pérot, G., and Guisnet, M., *in* "Zeolites, Facts, Figures, Future" (P. A. Jacobs and R. A. van Santen, Eds.), Studies in Surface Science and Catalysis, Vol. 49, p. 1339. Elsevier, Amsterdam, 1989]
11. Weitkamp, J., and Ernst, S., *Catal. Today* **3**, 451 (1987).
12. Campelo, J. M., Lafont, F., and Marinas, J. M., *J. Catal.* **156**, 11 (1995).
13. Satterfield, Ch. N., "Heterogeneous Catalysis In Practice." McGraw–Hill, New York, 1980.
14. Gielgens, L. H., Veenstra, I. H. E., Ponec, V., Haanepen, M. J., and van Hooff, J. H. C., *Catal. Lett.* **32**, 195 (1995).
15. Arias, D., Campos, I., Escalante, D., Goldwasser, J., López, C. M., Machado, F. J., Méndez, B., Moronta, D., Pinto, M., Sazo, V., and Ramírez de Agudelo, M. M., *J. Mol. Catal.* **122**, 175 (1997).
16. Zubowa, H.-L., Richter, M., Roost, U., Parlitz, B., and Fricke, R., *Catal. Lett.* **19**, 67 (1993).
17. Yang, S. M., Guo, D. H., Lin, J. S., and Wang, G. T., *in* "Zeolites and Related Microporous Materials: State of the Art 1994" (J. Weitkamp,

H. G. Karge, H. Pfeifer, and W. Hölderich, Eds.), Studies in Surface Science and Catalysis, Vol. 84, p. 1677. Elsevier, Amsterdam, 1994.
18. Escalante, D., López, C. M., Machado, F, J., Matjushing, M., Méndez, B., Pinto, M., and Ramírez-Agudelo, M. M., *in* "Environmental Catalysis" (G. Centi, C. Cristiani, P. Forzatti, and S. Perathoner, Eds.), p. 415. SCI Pub., Rome, 1995.
19. Escalante, D., Goldwasser, J., López, C. M., Machado, F. J., Pinto, M., and Ramírez-Agudelo, M. M., *in* "Proceedings of the XV Iberoamerican Symposium on Catalysis" (E. Herrero, O. Anunziata, and C. Pérez, Eds.), Vol. 1, p. 103. Córdoba, Argentina, 1996.
20. Giraldo, L., Pfaff, C., López, C. M., Machado, F., Méndez, B., Goldwasser, J., Ramírez de Agudelo, M. M., Rondón, S., Houalla, M., and Hercules, D. M., *Surf. Interface Anal.* **24**, 863 (1996).
21. Escalante, D., Giraldo, L., Pinto, M., Pfaff, C., Sazo, V., Matjushin, M., Méndez, B., López, C. M., Machado, F. J., Goldwasser, J., and Ramírez de Agudelo, M. M., *J. Catal.* **169**, 176 (1997).
22. López, C. M., Machado, F. J., Goldwasser, J., Méndez, B., Rodríguez, K., and Ramírez de Agudelo, M. M., *Zeolites* **19**, 133 (1997).
23. Escalante, D., Méndez, B., Hernández, G., López, C. M., Machado, F. J., Goldwasser, J., and Ramírez de Agudelo, M. M., *Catal. Lett.* **47**, 229 (1997).
24. Akolekar, D. B., *J. Mol. Catal.* **104**, 95 (1995).
25. Alfonzo, M., Goldwasser, J., López, C. M., Machado, F. J., Matjushin, M., Méndez, B., and Ramírez de Agudelo, M. M., *J. Mol. Catal.* **98**, 35 (1995).
26. Van den Broek, A. C. M., van Grondelle, J., and van Santen, R. A., *J. Catal.* **167**, 417 (1997). [See references therein]
27. Sachtler, W. M. H., and Zhang, Z., *Adv. Catal.* **39**, 129 (1993).
28. Homeyer, S. T., and Sachtler, W. M. H., *J. Catal.* **117**, 91 (1989).
29. Goldwasser, J., Houalla, M., Fang, S. M., and Hall, W. K., *J. Catal.* **115**, 34 (1989).
30. Pantoja, A., Sarrín, J., González, L., Noguera, O., Pérez Zurita, M. J., Galavís, J. L., and Goldwasser, J., *J. Catal.* **142**, 110 (1993).
31. Goldwasser, M. R., Rojas, D., and Goldwasser, J., *J. Catal.* **135**, 596 (1992).
32. O'Rear, D. J., Loffler, D. G., and Boudart, M., *J. Catal.* **121**, 131 (1990).
33. Ponec, V., and Bond, G. C., Studies in Surface Science and Catalysis, Vol. 95, p. 371. Elsevier, Amsterdam, 1995.
34. Pérez Zurita, M. J., Vitale, G., Goldwasser, M. R., and Rojas, D., *J. Mol. Catal.* **107**, 175 (1996).
35. Segawa, K. I., and Hall, W. K., *J. Catal.* **76**, 133 (1982).
36. Flanigen, E. M., Lok, B. M. T., Patton, R. L., and Wilson, S. T., U.S. Patent 4,738,837 (1988).
37. Barrie, P. J., Smith, M., and Klinowski, J., *Chem. Phys. Lett.* **180**, 6 (1991).
38. Tapp, N., Milestone, N., Bowden, M., and Meinhold, R., *Zeolites* **10**, 105 (1990).
39. Kiviat, F. E., and Petrakis, L., *J. Phys. Chem.* **77**, 1232 (1973).
40. Campelo, J. M., Lafont, F., and Marinas, J. M., *Appl. Catal.* **152**, 53 (1997).
41. Sheppard, N., and Nguyen, T. T., *in* "Advances in Infrared and Raman Spectroscopy" (R. J. Clarke and R. E. Hester, Eds.), Vol. 4, p. 67. Wiley, New York, 1978.
42. Vaarkamp, M., Miller, J. T., Modica, F. S., and Koningsberger D. C., *J. Catal.* **163**, 294 (1996).
43. Kappers, M. J., and van der Maas, J. H., *Catal. Lett.* **10**, 365 (1991). [See references therein]
44. Corma, A., and Wojciechowski, B., *Catal. Rev. Sci. Eng.* **24**, 1 (1982).
45. Brouet, G., Chen, X., Lee, Ch. W., and Kevan, L., *J. Am. Chem. Soc.* **114**, 3720 (1992).
46. Brouet, G., Chen, X., and Kevan, L., *J. Phys. Chem.* **95**, 4928 (1991).
47. Olender (Levi), Z., Goldfarh, D., and Batista, J., *J. Am. Chem. Soc.* **115**, 1106 (1993).
48. Flanigen, E. M., Lok, B. M., Patton, R. L., and Wison, S. T., *in* "New Developments in Zeolite Science and Technology" (Y. Murakami, A. Lijima, and J. W. Ward, Eds.), p. 103. Elsevier, Amsterdam, 1986. [Wilson, S. T., and Flanigen, E. M., U.S. Patent 4,567,029 (1985)]
49. Anderson, J. R., and Avery, N. R., *J. Catal.* **5**, 446 (1966).
50. Sinfelt, J. H., Carter, J. L., and Yates, D. J. C., *J. Catal.* **24**, 283 (1972).
51. Anderson, J. R., "Chemisorption and Reactions on Metallic films," Vol. 2. Academic Press, London/New York, 1971. [See references therein]
52. Ponec, V., and Bond, G. C., Studies in Surface Science and Catalysis, Vol. 95, pp. 280, 437, 597. Elsevier, Amsterdam, 1995. [See references therein]
53. Arata, K., *Adv. Catal.* **37**, 165 (1990).
54. Tanabe, K., *Crit. Rev. Surf. Chem.* **1**, 1 (1990).
55. Soled, S. L., Gates, W. E., and Iglesia, E., U.S. Patent 5,422,327 (1995).
56. Szabo, J., Perrotey, J., Szabo, G., Duchet, J. C., and Cornet, D., *J. Mol. Catal.* **67**, 79 (1991).
57. Mooiweer, H. H., de Jong, K. P., Kraushaar-Czarnetzki, B., Stork, W. H. J., and Krutzen, B. C. H., *in* "Zeolites and Related Microporous Materials: State of the Art 1994" (J. Weitkamp, H. G. Karge, H. Pfeifer, and W. Hölderich, Eds.), Studies in Surface Science and Catalysis, Vol. 84, p. 2327. Elsevier, Amsterdam, 1994.
58. Guisnet, M., *Acc. Chem. Res.* **23**, 392 (1990).
59. Liu, H., Adeeva, V., Lei, G. D., and Sachtler, W. M. H., *J. Mol. Catal. A* **100**, 35 (1995).
60. Xu, B.-Q., and Sachtler, W. M. H., *J. Catal.* **167**, 224 (1997).
61. Liu, H., Lei, G. D., and Sachtler, W. M. H., *Appl. Catal.* **137**, 167 (1996).
62. Song, X., Reddy, K. R., and Sayari, A., *J. Catal.* **161**, 206 (1996).
63. Zarkalis, A. S., Hsu, C.-Y., and Gates, B. C., *Catal. Lett.* **29**, 235 (1994).
64. Adeeva, V., Lei, G. D., and Sachtler, W. M. H., *Appl. Catal.* **118**, L11–L15 (1996).